Incorporation of Inconel-718 material test data into material model input parameters for *MAT_224

Stefano Dolci[1], Kelly Carney[1], Leyu Wang[1], Paul Du Bois[2] and Cing-Dao Kan[1]

1Center for Collision Safety and Analysis, George Mason University, Fairfax, VA
2Consulting Engineer, Northville, MI

Abstract

A research team from George Mason University, Ohio State University, NASA and FAA has developed material data and analytical modeling that allows for precise input of material data into **LS-DYNA**® *using tabulation and the *MAT_224 material model. The input parameters of this model are based on data from many experimental coupon tests including tension, compression, impact, shear and biaxial stress states. The material model also includes temperature and strain rate effects.*

*This research effort involves the incorporation of the Inconel-718 material test data into the material model. This requires the development and validation of a set of material constants for this particular alloy, utilizing the tabulated input method of material model *MAT_224 in* **LS-DYNA** *with consideration given to strain rate and temperature.*

Alloy Inconel-718 is a precipitation hardenable nickel-based alloy designed to display exceptionally high yield, tensile and creep-rupture properties at temperatures up to 1300°F. The sluggish age-hardening response of alloy 718 permits annealing and welding without spontaneous hardening during heating and cooling. This alloy has been used for jet engine and high-speed airframe parts such as wheels, buckets, spacers, and high temperature bolts and fasteners.

**MAT_224 is an elastic-plastic material with arbitrary stress versus strain curve(s) and arbitrary strain rate dependency, all of which can be defined by the user. Thermo-mechanical and comprehensive plastic failure criterion can also be defined for the material. This requires a process of test data reduction, stability checks, and smoothness checks to insure the model input can reliably produce repeatable results. Desired curves are smooth and convex in the plastic region of the stress strain curves.*

Introduction

Inconel718 is an important engineering material widely used in aerospace applications. However, current constitutive models fall short in predicting the plastic and failure behavior of this material under various strain rates. One reason for this may be the high dependency of the properties of Inconel sheet on the manufacturing process and, hence, on the thickness of the sheet. This research effort, therefore, involves the development and validation of a set of material constants utilizing the tabulated input method of material model *MAT_224 in **LS-DYNA** with consideration given to strain rate and temperature, specifically for a rolled ½-inch Inconel-718 sheet. *MAT_224 is an elastic-plastic material model with arbitrary stress versus strain curve(s) and arbitrary strain rate dependency, all of which can be defined by the user. Thermo-mechanical and comprehensive plastic failure criterion can also be defined for the material. [1]
The deformation portion of the Inconel-718 *MAT_224 inputs are based on the results of uniaxial tensile testing conducted by Ohio State University [3][4][13] under plane stress conditions at varying strain rates and temperatures. Material model development and validation procedures are herein included as a reference for similar study.

Methodology

Many factors contribute to the variations of Inconel-718 measured material properties, including, but not limited to, the manufacturing and post-manufacturing processes, the test specimen orientation in regards to plate grain direction, etc. To minimize some of these discrepancies, the material studied here is Inconel-718 ½-inch plate manufactured by a sole company.
The ½-inch rolled plate metal Inconel-718 material is modeled using *MAT_224 in **LS-DYNA**. This is an isotropic elasto-thermo-visco-plastic constitutive relationship which states that stress is dependent on strain, strain rate and temperature:

$$\sigma_{ij} = \sigma_{ij}(\varepsilon_{ij}, \dot{\varepsilon}_{ij}, T)$$

Equation 1

Where σ_{ij} is stress, ε_{ij} is strain, $\dot{\varepsilon}_{ij}$ is the strain rate, and T is the temperature. In the elastic region, the Jaumann rate of the stress tensor, $\overset{\nabla}{\sigma}_{ij,}$ is obtained as a linear function of elastic strain rates; this is a generalization of hypo-elasticity:

$$\sigma_{ij}^{\nabla} = \lambda\left(\dot{\varepsilon}_{kk} - \dot{\varepsilon}_{kk}^{p}\right)\delta_{ij} + 2\mu\left(\dot{\varepsilon}_{ij} - \dot{\varepsilon}_{ij}^{p}\right)$$

Equation 2

Here $\dot{\varepsilon}^{p}_{ij}$ are the components of the plastic strain rate tensor and λ and μ are Lamé constants. Young's modulus, E, and Poisson's ratio, ν, may be converted by:

$$E = \frac{\mu(3\lambda + 2\mu)}{\lambda + \mu}$$

Equation 3

$$\nu = \frac{\lambda}{2(\lambda + \mu)}$$

Equation 4

The material response in the plastic region is determined by a von Mises-type yield surface in a six-dimension stress space that can expand and/or contract due to strain hardening, rate effects and thermal softening:

$$\sigma_{vm}\left(\sigma_{ij}\right) \le \sigma_y(\varepsilon_{ij}^p, \dot{\varepsilon}_{ij}^p, T) = \sigma_y(\varepsilon_{eff}^p, \dot{\varepsilon}_{eff}^p, T)$$

Equation 5

Where σ_{vm} is the von Mises stress, $\varepsilon^p{}_{eff}$ is the equivalent plastic strain and $\varepsilon^{\cdot p}{}_{eff}$ is the equivalent plastic strain rate. As the material is assumed isotropic, the dependency of the yield surface upon plastic strain and plastic strain rate can be expressed purely as a function of the second invariant of each tensor. Note that states on the yield surface are plastic, whereas states below the yield surface are elastic. Mathematically this is expressed as follows:

$$\sigma_{vm}\left(\sigma_{ij}\right) - \sigma_y(\varepsilon_{eff}^p, \dot{\varepsilon}_{eff}^p, T) \le 0$$

$$\dot{\varepsilon}_{eff}^p \ge 0$$

$$\dot{\varepsilon}_{eff}^p \cdot \left(\sigma_{vm}\left(\sigma_{ij}\right) - \sigma_y(\varepsilon_{eff}^p, \dot{\varepsilon}_{eff}^p, T)\right) = 0$$

Equation 6

The plastic strain rates are determined by associated flow leading to the well-known plastic incompressibility condition typical of metals:

$$\dot{\varepsilon}_{ij}^p = \dot{\varepsilon}_{eff}^p \frac{\partial \sigma_{vm}}{\partial \sigma_{ij}} \Rightarrow \sum_{k=1}^{3} \dot{\varepsilon}_{kk}^p \equiv 0$$

Equation 7

Common Elastic-Plastic Modeling Revisited

A review of common plastic material modeling procedures will demonstrate the limitations and error that can be introduced in the process. What follows is a detailed review, including typical assumptions, of the typical elastic-plastic material modeling procedure.

The material modeling begins with a standardized tensile test. A dog-bone specimen under a constant grip speed is pulled in a test machine (Figure 1). Two measurements are recorded, the force vs. time relationship, *F (t),* is measured with the tensile machine, and the displacement vs. time relationship, *D (t),* is measured by a gauge or an extensometer fixed to the specimen. The force vs. displacement curve is then generated by cross-plotting these two curves.

After acquiring the force vs. displacement curve, simple formulas are used to calculate engineering stress and engineering strain.

$$\sigma_{eng}\left(t\right) \equiv \frac{F\left(t\right)}{A_0}$$

$$\varepsilon_{eng}\left(t\right) \equiv \frac{L\left(t\right) - L_0}{L_0} = \frac{D\left(t\right)}{L_0}$$
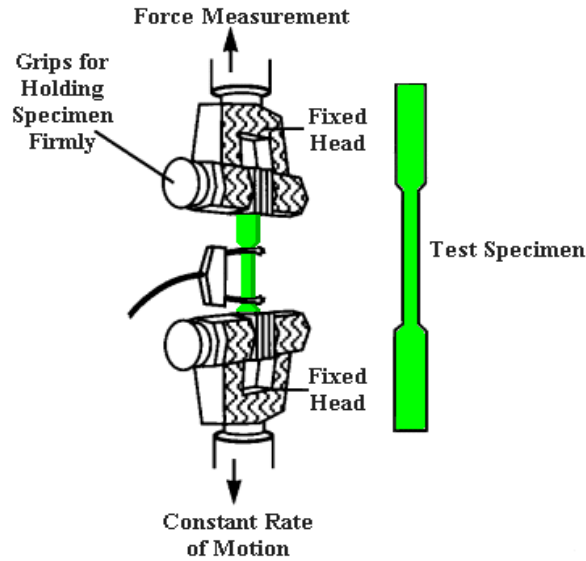
Equation 8

Figure 1 Standard Tensile Test [6]

Where $\sigma_{eng}(t)$ is the engineering stress vs. time relationship, ε_{eng} is the engineering strain, $F(t)$ is the force in the axial direction, A_0 is the original cross-sectional area, $L(t)$ is the instantaneous gauge length, L_0 is the original gauge length, and D is the displacement.

After knowing σ_{eng} and ε_{eng}, engineering stress may be converted into the true stress using the formula below .

$$\sigma = \sigma_{eng}(1 + \varepsilon_{eng})$$

Equation 9

Similarly, true strain may be converted by the following :

$$\varepsilon = \ln(\varepsilon_{eng} + 1)$$

Equation 10

In applying the formulas above, five assumptions have already been made:

Assumption 1: stress $\sigma_{ij}(t)$ is uniform over the mid cross-section of the specimen at any time.

Assumption 2: cross-sectional area is constant in the area measured by the extensometer.

Assumption 3: zero stress exists in the transverse and in the thickness direction.

Assumption 4: Strain components in the transversal and thickness directions are given as $-k\,\varepsilon_{11}$, where ε_{11} is longitudinal strain and k is close to 0.5

Assumption 5: strain is uniform in the area measured by the extensometer.

Any deviation from these assumptions will introduce errors in the derived stress-strain relationship. The final *MAT_224 Inconel-718 material model will use a Young's modulus of 210 GPa [7]. However, this value may not match all of the test data exactly. Therefore, when the hardening curves for the various test conditions are developed, a value that matches each specific test is adopted to enable the simulated hardening curve to start at the same point as the test curve. Starting at the same point is required in order to compare the fit of the hardening curve being developed. When the model is complete, the stress evolution follows the above modulus value up

to the proportional limit departure point for the different hardening curves, depending upon stress state, rate and temperature.

Traditionally, the yield stress is found by loading the specimen to just above the yield point and then unloading it completely, such that the remaining plastic strain under zero stress is 0.2%. As this approach can be both costly and time consuming, many practitioners simply find the slope of the elastic region and shift this line by 0.2% to the right. The intersection between this line and the stress strain curve is traditionally called the yield point (Figure 2). However, for **LS-DYNA** the elastic region corresponds to the linear portion of the strain-stress curve and the yield strength σ_Y needs to be defined as the end of the linear portion. The elastic part is modeled by giving two elastic material constants, Young's modulus, *E,* and Poisson's ratio, *ν.*
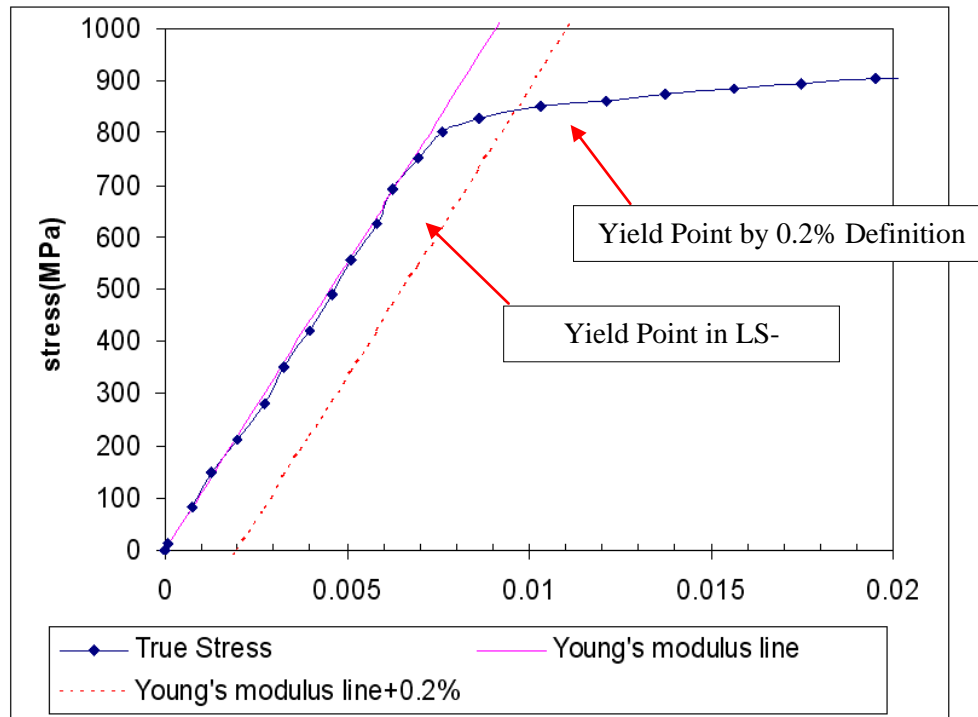

Figure 2: Finding Yield Stress by Shifting Elastic Region by 0.2%

For modeling the plastic region, the plastic strain, ε_p, is computed as:

$$\varepsilon_p \equiv \varepsilon - \sigma / E$$

Equation 11

After obtaining the plastic strain vs. stress relationship curve, input data are prepared for an **LS-DYNA** piecewise linear plasticity material model (*MAT_024). As shown in Figure 3, the stress value of the starting point of this curve has the same value as the stress at the proportional limit. This is critical to maintain a continuous transition between the elastic and plastic regions.

Under the assumptions that were previously mentioned, the load curve giving longitudinal stress versus longitudinal plastic strain is identical to the relationship between the effective plastic strain, ε^p_{eff}, and yield stress, σ_Y. This relation will be used to determine the deformation behavior after the elastic region.
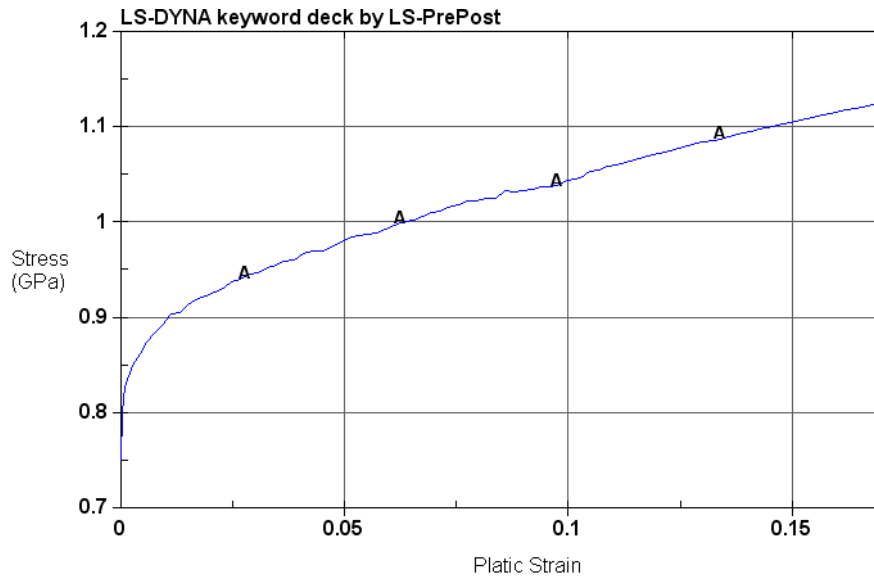
Figure 3: **LS-DYNA** Input Deck of a Piecewise Liner Plasticity Material Model (*MAT_024) of a Typical Test Result

Effective plastic strain, ε^p_{eff}, is a monotonically increasing scalar value. It is calculated incrementally as a function of $\varepsilon^{\cdot p}_{ij}$, the plastic component of the rate of deformation tensor. In tensorial notation, this is expressed as:

$$\varepsilon^p_{eff} = \int_{t=0}^{t1} d\varepsilon^p_{eff} = \int_0^t \sqrt{2/3 \dot{\varepsilon}^p_{ij} \cdot \dot{\varepsilon}^p_{ij}}\, dt$$

Equation 12

If plastic deformation occurs at constant volume then:

$$\dot{\varepsilon}^p_{ij} = \dot{\varepsilon}^p_{11} \begin{pmatrix} 1 & 0 & 0 \\ 0 & -0.5 & 0 \\ 0 & 0 & -0.5 \end{pmatrix} \Rightarrow \dot{\varepsilon}^p_{eff} = \dot{\varepsilon}^p_{11}$$

Equation 13

Additionally,

$$\varepsilon^p_{eff} = \int_{t=0}^{t1} d\varepsilon^p_{eff} = \int_0^t \dot{\varepsilon}^p_{11} dt = \varepsilon^p_{11}$$

Equation 14

The yield surface can be determined by Equation 2:

$$\sigma_{vm} \le \sigma_y = f_h\left(\varepsilon^p_{eff}\right)$$

Equation 15

Where $f_h\,(\varepsilon^p_{eff})$ is the tabulated input and $f_h(0)$ is the yield stress that denotes the value of f_h when $\varepsilon^p_{eff} = 0$ (the starting point of the plastic strain vs. stress curve).

The effective stress according to von Mises, σ_{vm}, is defined as follows:

$$\sigma_{vm} = \sqrt{\frac{1}{2}\left[(\sigma_x - \sigma_y)^2 + (\sigma_y - \sigma_z)^2 + (\sigma_z - \sigma_x)^2 + 6\sigma_{xy}^2 + 6\sigma_{yz}^2 + 6\sigma_{zx}^2\right]}$$

Equation 16

It can be observed that it is identical to the longitudinal stress under conditions of uniaxial tension:

$$\sigma_{ij} = \sigma_{11}\begin{pmatrix} 1 & 0 & 0 \\ 0 & 0 & 0 \\ 0 & 0 & 0 \end{pmatrix} \Rightarrow \sigma_{vm} = \sigma_{11} \ (\sigma_{11} > 0)$$

Equation 17

Violations of Common Assumptions

The common method for modeling elastic-plastic materials presented in the previous section is invalid after the necking point because at least three out of five assumptions are violated.

Assumption 1 is still considered valid because the stress $\sigma_{ij}(t)$ varies little over the cross-sectional area at any time.

Assumption 4 is still valid because the material remains isotropic and plastically incompressible after onset of the plastic instability.

Assumption 2 is invalid, as the cross-sectional area is much smaller in the localized region after necking and therefore not a constant in the region spanned by an extensometer.

Assumption 3 is invalid, as transversal stresses will develop after the onset of necking and additional stresses in the thickness direction will develop after the onset of local necking. Consequently, after necking the specimen is no longer in a uniaxial stress condition.

Before necking, under uniaxial stress conditions, the only non-zero stress component is the axial stress, σ_l:

$$\sigma = \begin{pmatrix} \sigma_l & 0 & 0 \\ 0 & 0 & 0 \\ 0 & 0 & 0 \end{pmatrix} \qquad \sigma_{vm} = \sigma_l$$

Equation 18

After necking, a transverse stress, σ_t, appears because the material will resist shrinking in the transverse direction:

$$\sigma = \begin{pmatrix} \sigma_l & 0 & 0 \\ 0 & \sigma_t & 0 \\ 0 & 0 & 0 \end{pmatrix} \qquad \sigma_{vm} \neq \sigma_l$$

Equation 19

As the local necking develops we see additional stresses in the thickness direction, σ_{tt}:

$$\sigma = \begin{pmatrix} \sigma_l & 0 & 0 \\ 0 & \sigma_t & 0 \\ 0 & 0 & \sigma_{tt} \end{pmatrix} \qquad \sigma_{vm} \neq \sigma_l$$

Equation 20

An accurate measurement of σ_l can be obtained by applying the instantaneous necking cross-sectional area (measured by digital imaging) in the stress calculation. It is, however, not possible

to measure the transverse stress, σ_t, nor the thickness stress, σ_{tt}. Therefore, σ_{vm} is generally unknown after necking. If the uniaxial stress assumption is still applied (assume $\sigma_{vm} \approx \sigma_t$ after necking) and this false von Mises stress vs. effective plastic strain relationship is used to define the behavior of material, then the simulation result will deviate from the real test.

Assumption 5 is invalid because the strain is not uniform within the measuring distance of the extensometer. After the onset of necking, the neck will have a higher strain than the rest of the part. An accurate measurement of strain the region of necking can be obtained via a digital image correlation (DIC).

Stress Strain Relationship after Necking

In order to create an accurate material model and simulate the tensile test in **LS-DYNA**, the method used is as follows: Start by estimating several post-necking plastic stress-strain curves as input by extrapolating the curve before necking. Then compare the simulation force vs. displacement curve with test results and pick the input curve that gives the closest match. Note that the complete specimen geometry must be precisely modeled by measuring the actual specimen, rather than using the design values on the blueprint. Also note that at this stage in the process, the strain rate effect is not considered in the simulation. Next, input a single stress-strain curve associated with a particular strain rate, thereby making the material model strain rate independent. In other words, at this point in the modeling process, the material model will behave the same no matter the loading speed, as long as inertia effects are sufficiently small. Because of this strain rate independence, the simulation can be performed with an arbitrary (higher) loading speed instead of the actual loading speed that was used in the test, allowing for a much shorter simulation time. To safely implement the method, one must run several simulations to determine a good artificial loading speed in the simulation (Figure 4).

The rate-independent material model will have a dynamic effect if loaded at a very high speed due to the inertia effects. Therefore, start with a high loading speed of 10 m/s and gradually reduce it to the point where further reduction no longer changes the results. Use that final speed for loading the simulation; in this case, it is 1 m/s.

The necking point is identified by making the assumption that necking occurs at maximum load . The necking point is given by the intersection between the true strain versus true stress curve and its own derivative. So necking occurs where the true stress is equal to the tangent modulus:

$$\begin{cases} \sigma = \sigma(\varepsilon) \\ \sigma = \dfrac{d\sigma}{d\varepsilon} \end{cases}$$

<div align="right">Equation 21</div>

The hardening curves are extrapolated after necking using the following formula:

$$\sigma = k\left[\varepsilon_e + \varepsilon_p\right]^n$$

<div align="right">Equation 22</div>

Where k, ε_e, and n are fitting parameters and the exponent n is expected to vary between 0 and 1 as the hardening curve is expected to be monotonically increasing and to have a monotonically decreasing tangent.

After the necking point is determined, only the part of the strain-stress curve before necking is used for further processing (Figure 5).
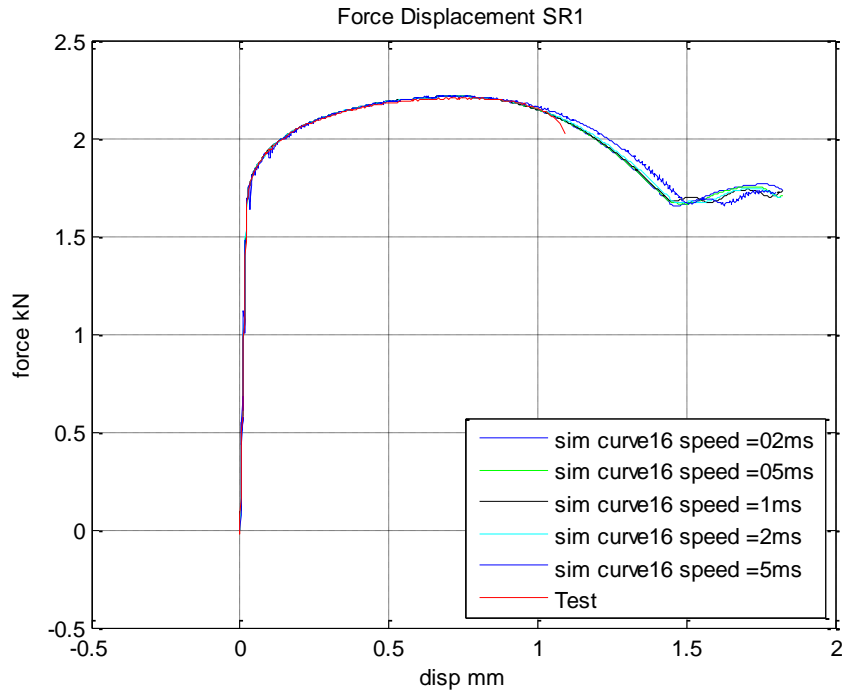
Figure 4: Artificial Loading Speed Determinations of a Typical Test Result
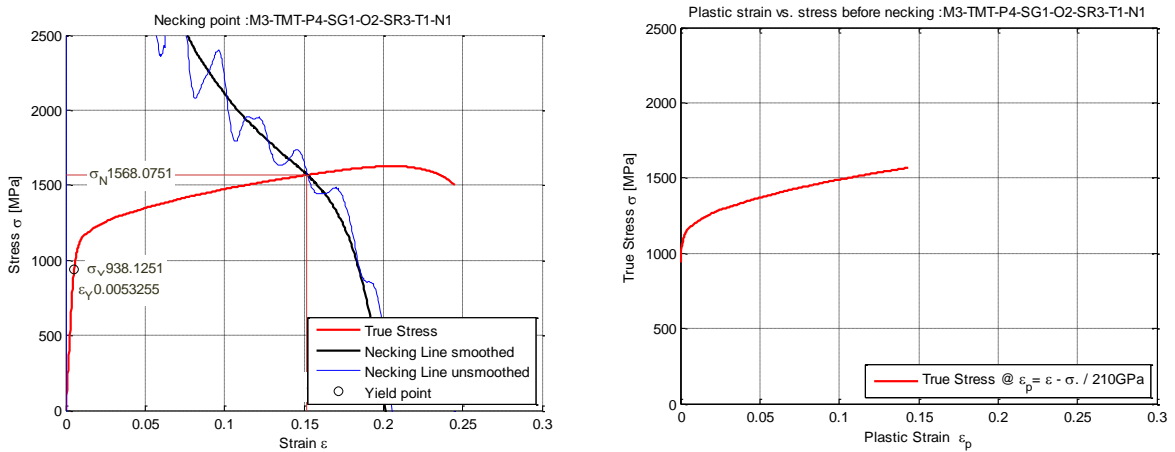

Figure 5: Left: Necking Judgment Line and Stress Strain Curve. Right: Stress Strain Curve after Trimming.

At the necking point, this curve should be continuous:

$$A \equiv \sigma\big|_{\varepsilon=\varepsilon 0}, \; B \equiv \varepsilon\big|_{\varepsilon=\varepsilon 0}$$

Equation 23

And smooth:

$$A \equiv \sigma\big|_{\varepsilon=\varepsilon 0}, \; C \equiv \frac{d\sigma}{d\varepsilon}\bigg|_{\varepsilon=\varepsilon 0}$$

Equation 24

Where A is the stress at necking, $B \equiv \varepsilon_0$ is the plastic strain at necking, and C is the slope (hardening modulus) at necking. Notice that there are three variables but only two boundary conditions. Therefore, the extrapolation is not uniquely defined and one of the three parameters can be freely chosen; as it has a bounded domain, it is typical to choose the exponent, *n*. Given a specific *n* value, ε_e and *k* are determined from the following relationships:

$$k = A\left(\frac{An}{C}\right)^{-n}$$

$$\varepsilon_e = \frac{An}{C} - B$$

Equation 25

After assuming different *n* values, a cluster of curves can be generated (Figure 6).
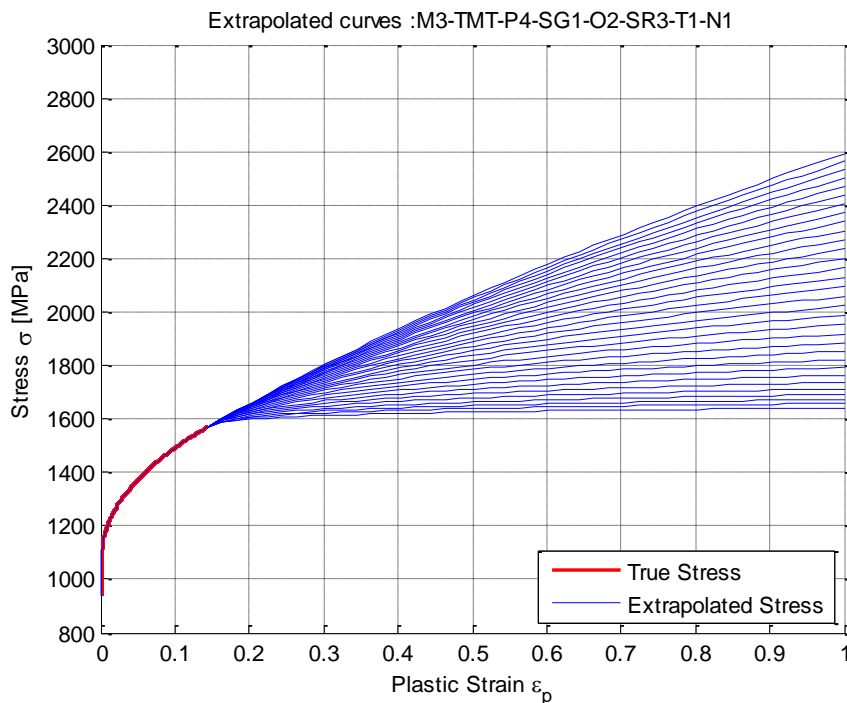
Figure 6: Extrapolated Curves after Necking Point

Several candidate curves were chosen from the generated plastic strain vs. stress curves (Figure 6) and these curves were input into the material model to simulate a tensile test. **Error! Reference source not found.** shows the force displacement curves obtained by two simulations overlaid with the real-life tensile test result. The curve 16 predicts a force displacement curve very close to the test. Therefore this curve is a good estimation of plastic strain vs. stress relationship.

As a supplementary evaluation, the 1st principal plastic strain contour at failure of the simulation is compared with the longitudinal strain digital image correlation data in the physical test. These two contours must be relatively similar to justify the estimated stress-strain relationship curve (Figure 8).
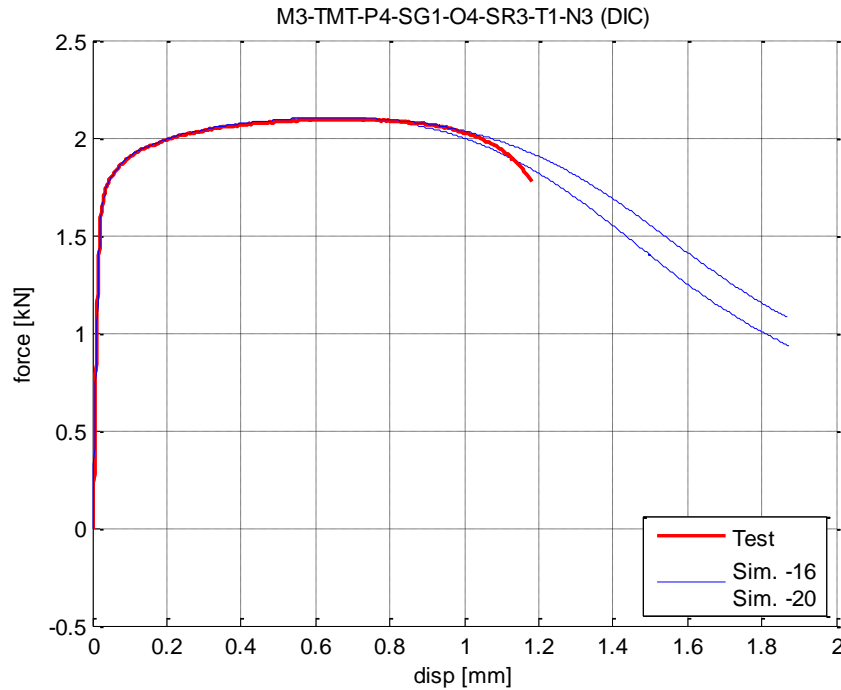
Figure 7: Force Displacement Result of Tensile Test Simulations with Different Hardening Curve Inputs
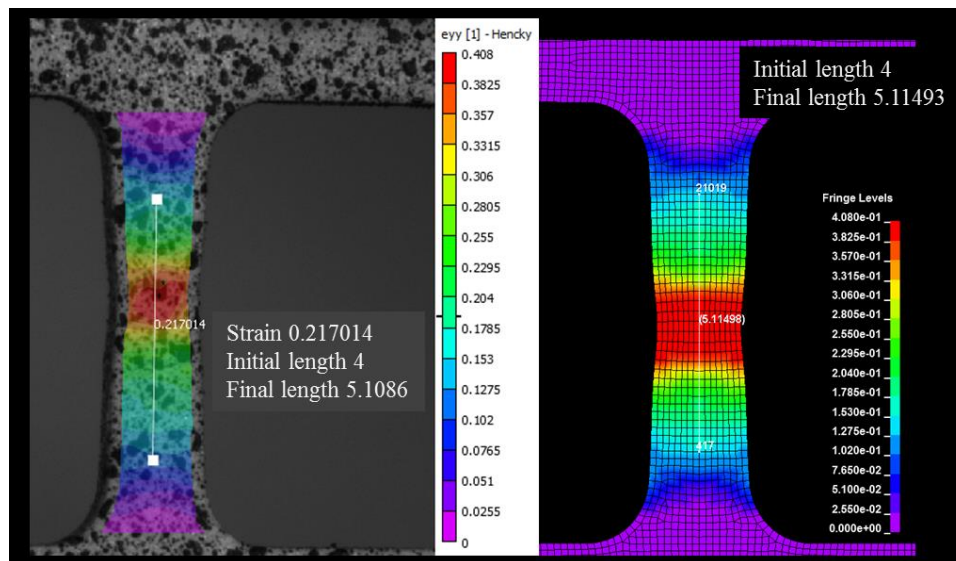

Figure 8: First Principal Plastic Strain Contour at Failure Comparison

The process described above in this section takes the raw data and smooths it to ensure that the analysis will properly converge and execute. It also avoids using the erroneous assumptions described previously. The input data developed in this process matches the actual test data as closely as possible, while removing high frequency oscillations and negative slope areas that could cause convergence problems.

Isothermal Effects

The method described above is valid for all quasi-static, isothermal, uniaxial tensile tests, independent of the temperature at which they were performed. The quasi-static testing must be performed at a low enough strain rate such that the process is isothermal and no thermo-mechanical coupling occurs during the experiment. Then the yield curve obtained by the process described earlier can be assigned to the specific temperature at which the test was conducted, which is necessary, as *MAT_224 requires an isothermal input curve.

In this way, a table of isothermal, temperature-dependent yield curves can be created by individually simulating all high- and low-temperature tensile tests for a given strain rate, without considering any thermal coupling in the simulations. That table can then be used (in conjunction with the table of rate-dependent yield curves) as input for simulations of dynamic experiments in which thermal effects and strain rate effects occur simultaneously and interact with each other.

Strain Rate Dependency Tabulated Input

Rolled Inconel 718 plate has a strain rate and temperature dependency in the plastic region.

$$\sigma_{ij} = \sigma_{ij}(\varepsilon_{ij}, \dot{\varepsilon}_{ij}, T)$$

<div align="right">Equation 26</div>

Multiple tensile tests were conducted using different strain rates. Each of the different strain rate tests was processed using the method described previously. The end result is shown in Figure 7; each curve represents the plastic strain vs. stress relationship corresponding to a particular strain rate.
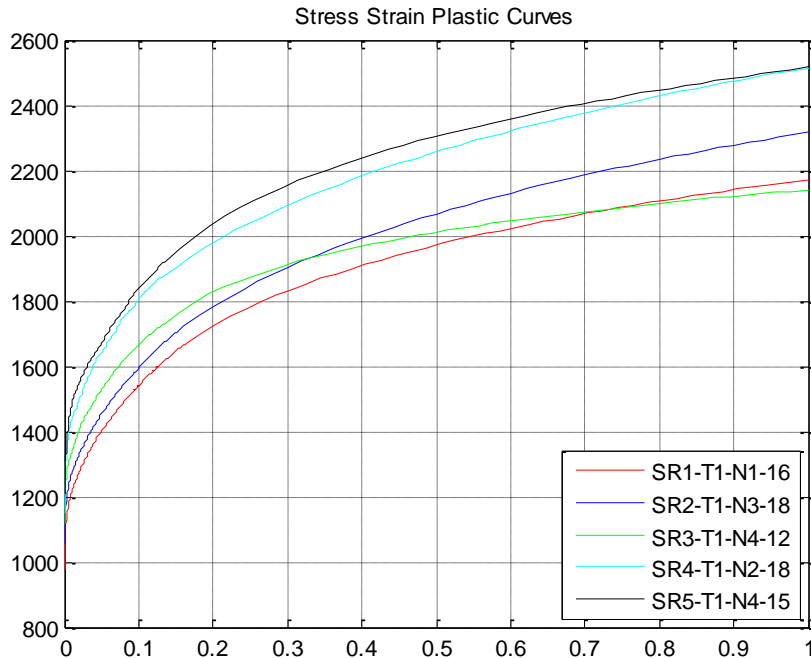

Figure 7: Plastic Strain, Stress Relationship of Rolled Inconel-718 Sheet under Different Strain Rates

Strain Rate Is Not a Constant

Initially, the strain rate is assumed to be either the nominal strain rate of the test, or the grip speed divided by the initial length of the sample covered by the extensometer. However, this assumption is incorrect, and there are two reasons. First, it is easy to show that:

$$\frac{d\varepsilon}{dt}(t) = \frac{1}{l(t)}\frac{dl}{dt}$$

Equation 27

Consequently, the strain rate is not constant under constant grip loading speed. Although the strain rate is uniform over the sample until necking occurs, it varies (decreases) with time if the grip speed is constant.

Second, after the onset of necking, all plastic deformation will localize in the necked area, whereas the plastic strain will remain constant outside the neck. Therefore, after necking, the strain rate will increase in the necked area and will no longer be uniform over the sample:

As shown in , within the gauge length L_0, the specimen is uniformly deformed before necking. After necking, the deformation is localized. Only a small piece of material at the necking point undergoes further deformation while the material elsewhere remains at constant plastic strain.
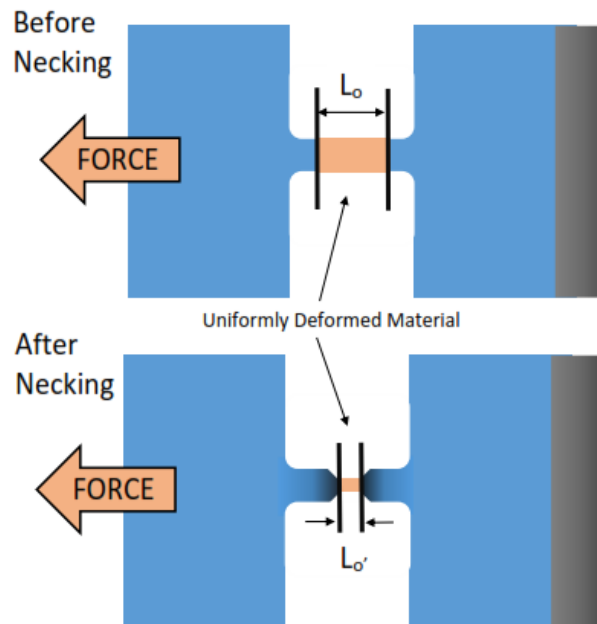

Figure 8: Length of Uniformed Deformed Material is Much Shorter after Necking

Assuming the deformation at the necking point is still uniform over a smaller distance L_0', then the engineering strain rate before necking is:

$$\dot{\varepsilon}_{eng\_bf\_necking} = \frac{\dot{L}(t)}{L_0}$$

Equation 28

Whereas the engineering strain rate after necking is:

$$\dot{\varepsilon}_{eng\_af\_necking} = \frac{\dot{L}(t)}{L_0'}$$

<div align="right">Equation 29</div>

And consequently it is shown that the engineering strain rate will increase considerably in the necked area:

$$\because L_0' << L_0$$

$$\therefore \dot{\varepsilon}_{eng\_af\_necking} > \dot{\varepsilon}_{eng\_bf\_necking}$$

<div align="right">Equation 30</div>

The same tendency is true for the true strain rate, although somewhat more difficult to show. Other variations in the testing procedure (e.g. non-constant grip speed, non-fixed boundary conditions, etc.) may also influence the strain rate value and cause the nominal strain rate to deviate from the physical value. Therefore, the measured displacement time history from the test must be input into the numerical model to accurately simulate the strain rates that occurred in each test.

High Strain Rate Sensitivity

As described in the previous section, the strain rate in a test with localization is not a constant. Localization is especially early and extreme in the higher strain rate Inconel-718 tests. The strain rate in the region of localization may reach values significantly above the nominal strain rate for the specimen. As a result, tension test data must be supplemented with synthetic curves generated using rate sensitivity trends from tension and compression tests. The compression tests reached much higher strain rates than the tension test but, due to friction and boundary conditions, complete stress-strain curves are difficult to derive from compression tests. Therefore, synthetic curves are created using a combination of information from the compression and tension tests. These synthetic curves are combined with the stress-strain curves derived directly from the tension tests. The tests referenced below were performed by Ohio State University. [13] Looking at the stress at a particular strain (specifically, 5% strain) across all tests categorized by differing strain rates demonstrates the strain rate sensitivity (**Error! Reference source not found.**). As shown in **Error! Reference source not found.**, at any given strain rate, there is a fairly wide spread between the stresses from the compression series and the tension test series. The strain rate abscissa is plotted on a logarithmic scale. The compression tests were translated so that their stresses passed through the tension tests of the ½-inch plate. The strain rate sensitivity is shown to conform to the theory that the yield strength increases as a logarithmic function of strain rate between rates of $\sim 10^{-4}$ s^{-1} and $\sim 10^3$ s^{-1}, and at strain rates greater than $\sim 10^3$ s^{-1} the stress increases as a linear function of the increase in strain rate, due to a change in the physical processes causing the change. [8]

The initial curve fit is (y = 25.1413 ln (x) +1508.252 for the lower strain rates and y = .10144 x + 1450.415 for the higher strain rates). In tension tests conducted at the nominal strain rate higher than $\sim 10^3$ s^{-1} the physical processes causing the strain rate sensitive behavior of the material at these intermediate rates is transitioning, and is a combination of both the lower and higher rate physics. As a result, the exact stress-strain behavior can neither be obtained by extrapolation, nor by reading it directly from the tests. The initial sensitivity curve created using the two separated curve fitting is shown in **Error! Reference source not found.**. As mentioned before, the stress-strain curves required by *MAT_224 must be isothermal. The tests at the higher strain rates were not at a constant strain rate and not isothermal; this is another reason why synthetic stress-strain curves were required. The stress-strain curve generated for the 1E-4 s^{-1} rate was used as the basis for all of the synthetic higher rate curves. Each curve's stress was translated so that its value at 5% strain was at the desired value. These curves were bundled together as a tabulated input for *MAT_224 [1]. Intermediate curves are created internally by **LS-DYNA** through linear interpolation between user input curves. Unlike material models which use curve-fitting to fit an

analytical formula to the test data and derive values for material constants, this method reads all of the input curves and precisely generates an internal yield surface numerically. The strain rate sensitivity and consequently the iso-rate curves table was established by trial-and-error matching of the tension test data.
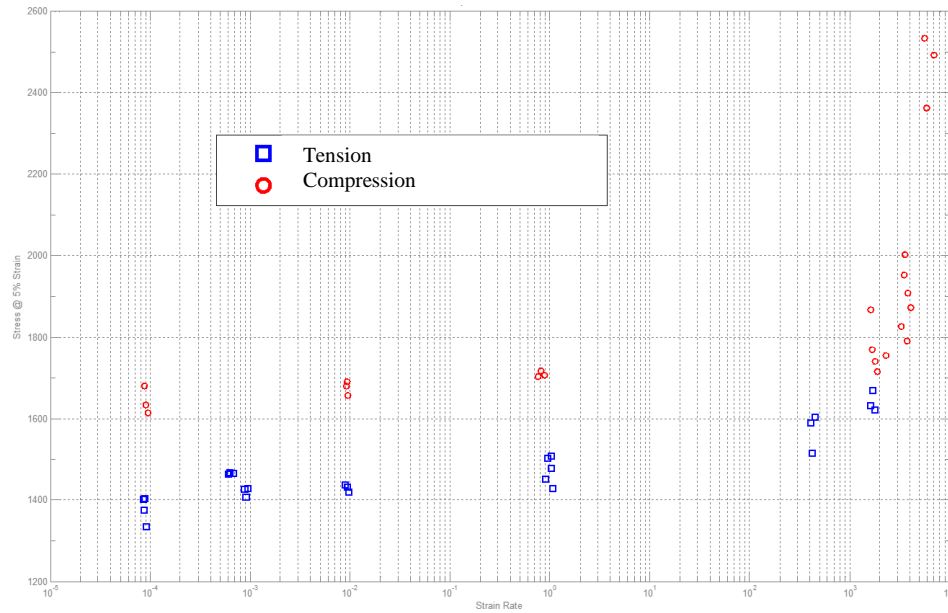

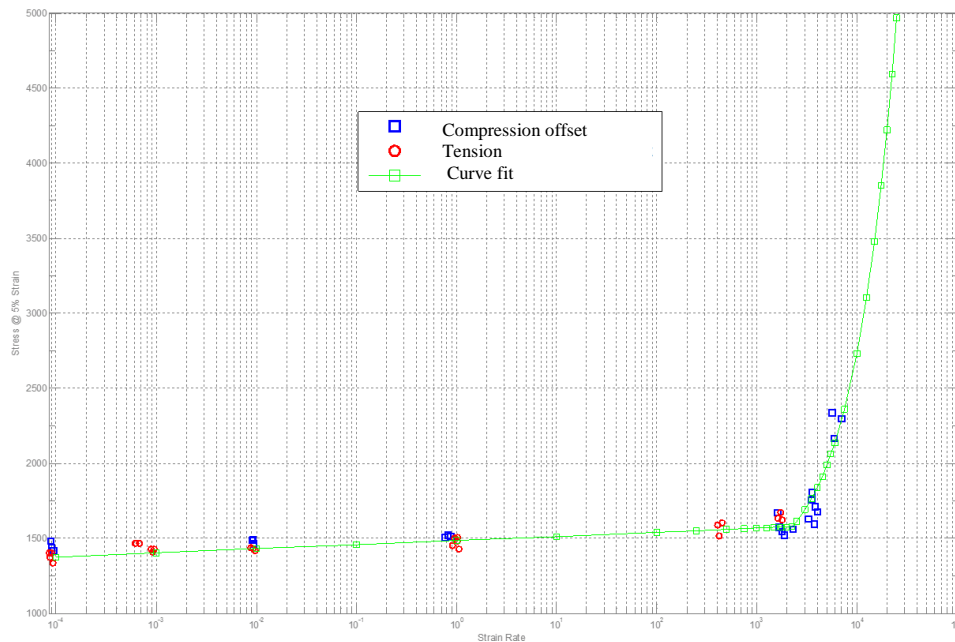Figure 9: Stress at 5% Strain – All Tests.

Figure 10: Stress at 5% Strain – Global data curve fit.

Conversion of Plastic Work into Heat (Taylor-Quinney Effect)

In the higher rate tests within the localized region of necking, there is not sufficient time for conduction to carry away the heat generated by the plastic deformation, and so the process becomes adiabatic. This adiabatic process causes a significant increase in the temperature of the specimen locally and governs the behavior at larger strains. As a result, the simulation of the tension tests is sensitive to the amount of energy generated by the plastic work, which is converted into thermal energy.

The percentage of plastic work that is converted into thermal energy is defined by the Taylor-Quinney coefficient, typically signified as *β*. Research by Ravichandran [9] and Rosakis **Error! Reference source not found.** yielded values for the Taylor-Quinney coefficient for α-titanium which were not constant, but were a function of both strain rate and, to a lesser extent, plastic strain. Additionally, [9] and **Error! Reference source not found.** also present variable values of *β*'s for Al2024, which are a strong function of plastic strain. The capability to input a variable *β* in *MAT_224 is available, but no published data for the Taylor-Quinney coefficient for Inconel-718 is available. Independent measurements of temperature rise in high rate deformation are planned by OSU, but are not yet available. Therefore, a constant *β* value of .8, which best matched the stress-strain test behavior exhibited in the tension tests, was determined through trial-and-error.

With this information, a fully coupled thermal solution using *MAT_224 in **LS-DYNA** could be performed. This simulates the conduction of thermal energy away from highly strained elements. Without including conduction, temperatures will rise more in the simulations than in tests, leading to non-physical analytical results. This non-physical result will be very small in high rate, short duration simulations, and can be safely ignored. In simulations where both high rate and low rate loading takes place simultaneously and significant strains are introduced into elements at a lower rate (i.e. longer duration simulation, such as full engine blade loss) as well as at high rates, including conduction may be required for accurate analysis.

Material Model Creation by Simulation of Mechanical Property Tests
Test Data

The test data includes time, force and displacement information. Every test comes with a CAD image showing the exact specimen dimensions from measurement. A DIC imagine taken at the time of failure (the last data point of the test data) is also included. The tests in Table 1 are provided by Ohio State University [13].

Test Series	Test Name	Nominal Strain Rate (1/s)	Apparatus	Plate Stock	Specimen Geometry	Specimen Orientation	Temp (°C)
Tension Strain Rate Dependence	M3-TMT-P4-SG1-O1-SR1-T1-N1	1.00E-04	Instron	0.5"	Flat Dogbone	Rolled	RT
	M3-TMT-P4-SG1-O1-SR1-T1-N2						
	M3-TMT-P4-SG1-O1-SR1-T1-N3						
	M3-TMT-P4-SG1-O1-SR1-T1-N4						
	M3-TMT-P4-SG1-O1-SR2-T1-N1	1.00E-02					
	M3-TMT-P4-SG1-O1-SR2-T1-N2						
	M3-TMT-P4-SG1-O1-SR2-T1-N3						
	M3-TMT-P4-SG1-O1-SR3-T1-N1	1.00E+00					
	M3-TMT-P4-SG1-O1-SR3-T1-N3						
	M3-TMT-P4-SG1-O1-SR3-T1-N4						
	M3-TMT-P4-SG1-O1-SR3-T1-N6						
	M3-TMT-P4-SG1-O1-SR3-T1-N7						
	M3-TMT-P4-SG1-O1-SR4-T1-N2	5.00E+02	SHB				
	M3-TMT-P4-SG1-O1-SR4-T1-N4						
	M3-TMT-P4-SG1-O1-SR4-T1-N5						
	M3-TMT-P4-SG1-O1-SR5-T1-N3	2.00E+03					
	M3-TMT-P4-SG1-O1-SR5-T1-N4						
	M3-TMT-P4-SG1-O1-SR5-T1-N5						

Test Series	Test Name	Nominal Strain Rate (1/s)	Plate Stock	Specimen Geometry	Specimen Orientation	Temp (°C)
Compression Strain Rate Dependence	M3-TMC-P4-SG1-O1-SR1-T1-N1	1.00E-04	0.5"	Flat Dogbone	Rolled	RT
	M3-TMC-P4-SG1-O1-SR1-T1-N2					
	M3-TMC-P4-SG1-O1-SR1-T1-N3					
	M3-TMC-P4-SG1-O1-SR2-T1-N1	1.00E-02				
	M3-TMC-P4-SG1-O1-SR2-T1-N2					
	M3-TMC-P4-SG1-O1-SR2-T1-N3					
	M3-TMC-P4-SG1-O1-SR3-T1-N1	1.00E+00				
	M3-TMC-P4-SG1-O1-SR3-T1-N2					
	M3-TMC-P4-SG1-O1-SR3-T1-N3					
	M3-TMC-P4-SG1-O1-SR4-T1-N2	1.00E+03				
	M3-TMC-P4-SG1-O1-SR4-T1-N3					
	M3-TMC-P4-SG1-O1-SR4-T1-N5					
	M3-TMC-P4-SG1-O1-SR4-T1-N10					
	M3-TMC-P4-SG1-O1-SR4-T1-N11					
	M3-TMC-P4-SG1-O1-SR5-T1-N1	2.00E+03				
	M3-TMC-P4-SG1-O1-SR5-T1-N2					
	M3-TMC-P4-SG1-O1-SR5-T1-N3					
	M3-TMC-P4-SG1-O1-SR5-T1-N4					
	M3-TMC-P4-SG1-O1-SR5-T1-N5					
	M3-TMC-P4-SG1-O1-SR5-T1-N6					
	M3-TMC-P4-SG1-O1-SR7-T1-N1	5.00E+3				
	M3-TMC-P4-SG1-O1-SR7-T1-N2					
	M3-TMC-P4-SG1-O1-SR7-T1-N3					

Test Series	Test Name	Strain Rate (1/s)	Apparatus	Plate Stock	Specimen Geometry	Specimen Orientation	Temp (°C)
Temperature Dependence	M3-TMT-P4-SG1-O1-SR6-T1-N1	1.00E-03	Instron	0.5"	Flat Dogbone	Rolled	RT
	M3-TMT-P4-SG1-O1-SR6-T1-N2						
	M3-TMT-P4-SG1-O1-SR6-T1-N3						
	M3-TMT-P4-SG1-O1-SR6-T2-N1						200
	M3-TMT-P4-SG1-O1-SR6-T2-N3						
	M3-TMT-P4-SG1-O1-SR6-T2-N4						
	M3-TMT-P4-SG1-O1-SR6-T3-N1						400
	M3-TMT-P4-SG1-O1-SR6-T3-N2						
	M3-TMT-P4-SG1-O1-SR6-T3-N3						
	M3-TMT-P4-SG1-O1-SR6-T4-N1						600
	M3-TMT-P4-SG1-O1-SR6-T4-N2						
	M3-TMT-P4-SG1-O1-SR6-T4-N3						
	M3-TMT-P4-SG1-O1-SR6-T5-N1						800
	M3-TMT-P4-SG1-O1-SR6-T5-N2						
	M3-TMT-P4-SG1-O1-SR6-T5-N3						

Table 1: Tests Series Provided by Ohio State University

Temperature Effect

Fifteen tests measuring the temperature effect of the material are listed in the lower part of Table 1. Besides the room temperature tests, four additional temperature groups were selected: , 200°C, 400°C, 600°C and 800°C.

The temperature effect was studied with input decks for *MAT_224 based on single hardening curves at the test rate of 1E-3 s^{-1}. All of the thermal tests were conducted at this rate. Use of a single stress-strain curve creates a strain rate insensitive analysis and allows the displacement to be applied at an artificially high grip speed of 1 m/s.

In these models the sample dimensions match the corresponding test specimen precisely.

Stress Strain Relationship at Room Temperature

Three tests at room temperature and strain rate 1E-3 s^{-1} are listed in **Error! Reference source not found.**. M3-TMT-P4-SG1-O1-SR6-T1-N2 was selected to represent this group of data and undergo further processing. The engineering strain vs. stress relationship was derived using Equation 8 and following the procedure introduced before, the true stress-strain relationship is reconstructed.

By applying Equation 11 and adopting a Young's modulus of 210.0 GPa, the plastic strain vs. stress relationship was calculated. To determine the necking point, the true strain vs. stress curve was smoothed and subsequently Equation 24 and Equation 25 (differentiation stress with respect to strain) were used to obtain the tangent modulus curve. Another smoothing was performed on the tangent modulus curve, and the intersection between these two lines defines the necking point, as shown by Figure . The true stress and true strain at necking were recorded. Corresponding plastic strain at necking was evaluated using Equation 21 and only the part of the hardening curve before necking was kept. By applying Equation 22, the hardening curve was extrapolated beyond necking.
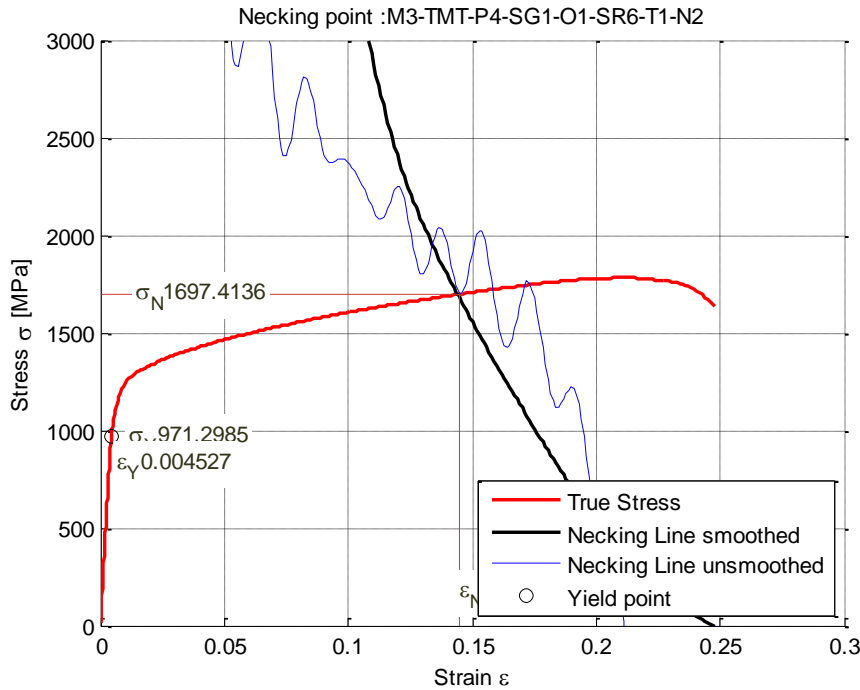
Figure 13: True Stress Strain Relationship and Necking Point Judgment of Strain Rate = 1E-3 s^{-1}

A total of 64 curves were generated by varying the exponent *n* (Figure). The remaining two parameters, ε_e and *k,* were calculated using Equation 25. Extrapolation was performed using MatLab. Each of the generated hardening curves was used in an **LS-DYNA** *MAT_224 input deck simulating the tensile test. In this model, the sample dimensions match the sample of test M3-TMT-P4-SG1-O1-SR6-T1-N2 exactly.
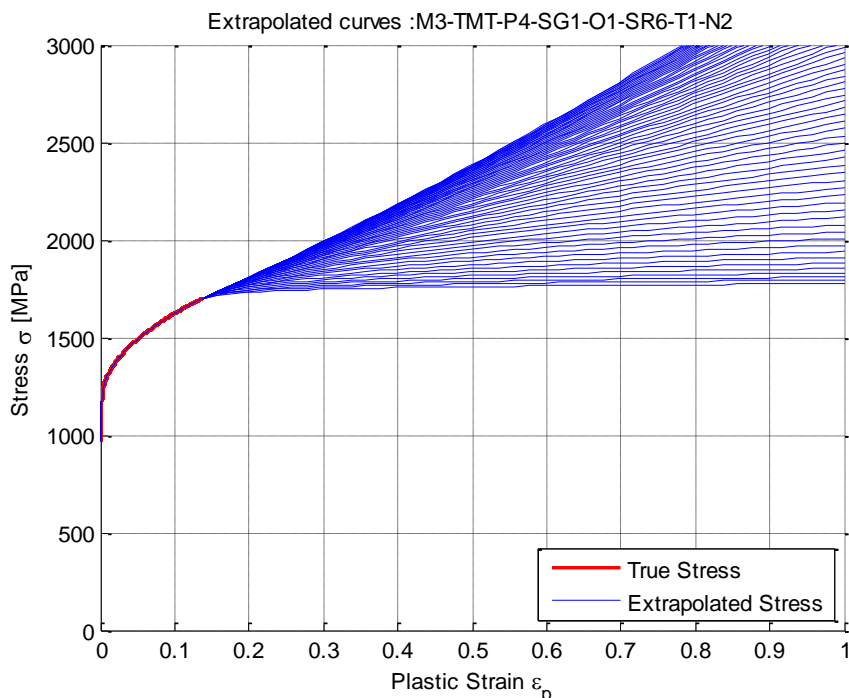

Figure 14: Plastic Strain vs. Stress Relationship of Strain Rate = 1 s^{-1}

A DATABASE_CROSS_SECTION was defined to measure the cross-sectional force. Two nodal points corresponding to the base points of the extensometer are stored in the NODOUT file. The difference in z displacement of these two nodal points gives the elongation of the extensometer as predicted in the simulation. The measuring nodes have an initial distance of 4mm. The cross-section for force measurement is located at the center of the specimen. A cross-plot of this elongation with the cross-sectional force can be directly compared to the force displacement curve form the test. This simulation is performed repeatedly for all the extrapolated candidate input curves until one of them matches the force displacement response of the test. The stress-strain curve number 24 gives the best match, as demonstrated in Figure .

In Figure 16, a simulation contour of 1st principal strain is compared to the DIC image from the test at the time right before failure and the result yields good agreement.
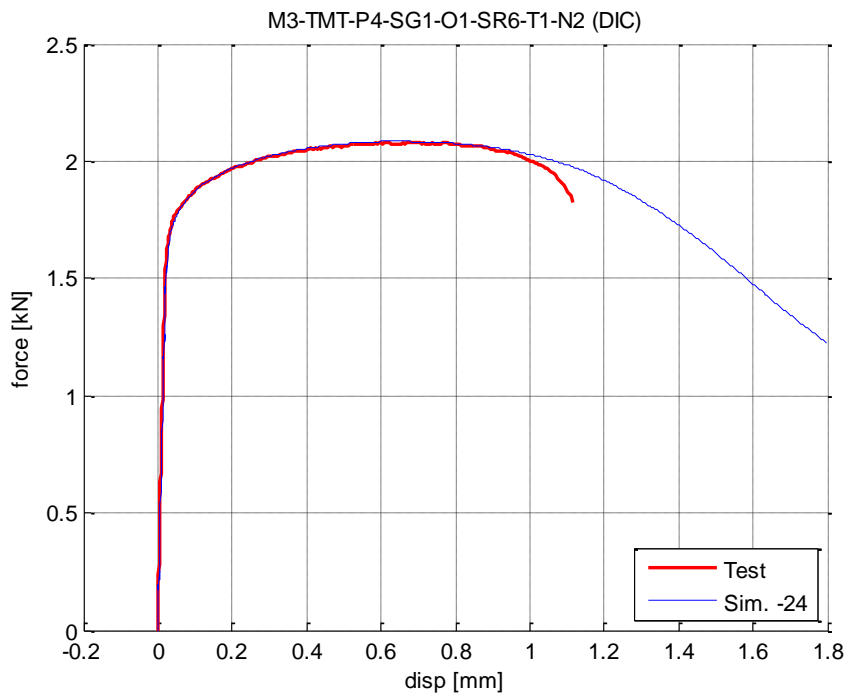
Figure 15: Force Displacement Result, Curve #24
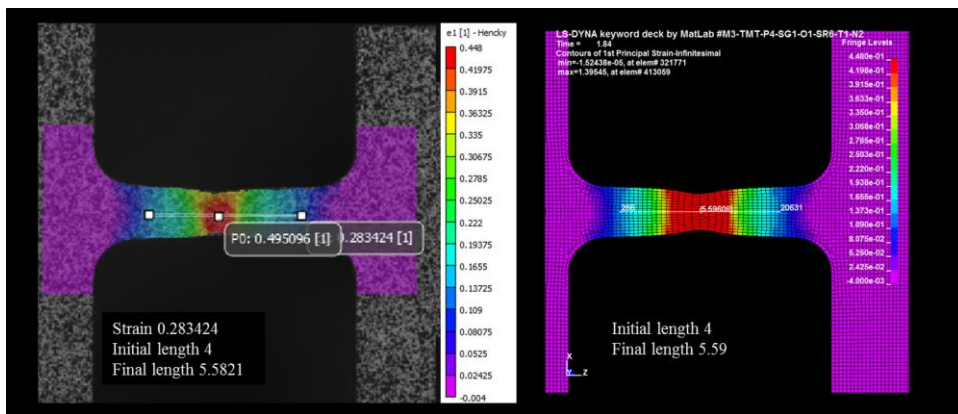
Figure 16: Left: Plastic Strain DIC Image Immediately Before Failure
Right: 1st Principal Strain Simulation Contour Immediately Before Failure Time
[Test: M3-TMT-P4-SG1-O1-SR6-T1-N2; Strain Rate = 1E-3 s^{-1}]

Stress Strain Relationship at Other Temperatures

By applying the same curve extrapolation and selection method used in the previous section, isothermal, temperature-dependent stress-strain curves were generated (Figure).An extra artificial curve at constant stress zero was added at Inconel melting temperature.
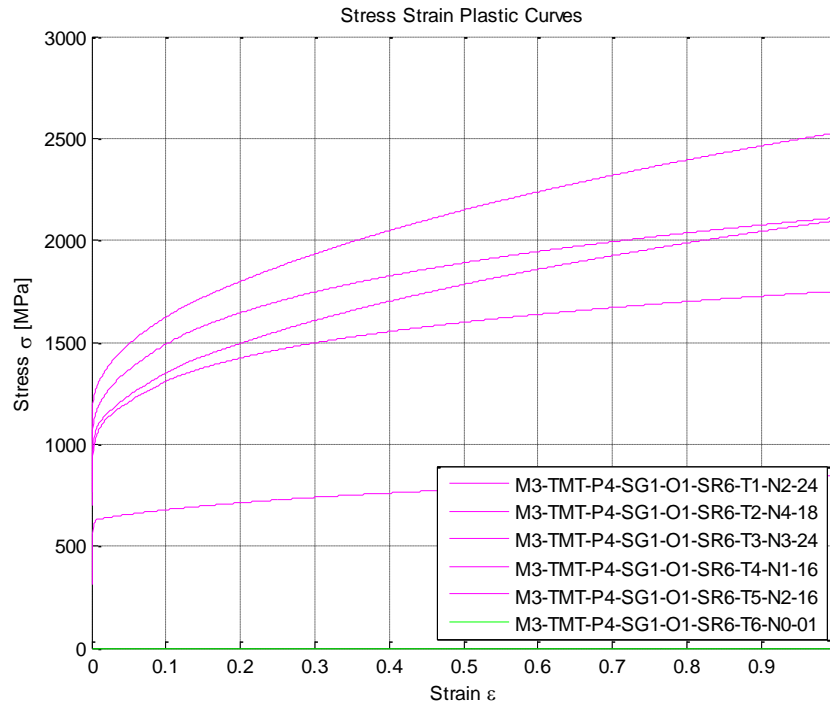

Figure 17: Temperature Dependency Input Curves

Stress Strain Relationship at Single Varying Strain Rates

A hardening curve was derived for each strain rate from the "Tension Strain Rate Dependence" series of Table 1. For the lower strain rates flat dog-bone specimens were pulled at room temperature on the Instron machine. Displacement and force were measured at a fixed time interval. All simulations were performed with an arbitrary loading speed of 1m/s.
The testing at higher strain rates was performed as described in [13], a method commonly referred to as a split-Hopkinson bar. This method differs from the dog-bone specimen tension testing in that the specimen undergoes impulsive loading, rather than being machine-loaded following a prescribed path, and therefore higher strain rates can be achieved.

Stress Strain Relationship of Strain Rate = 1E-4 S^{-1}

The three quasi-static tests at strain rate 1E-4 s^{-1} are listed in **Error! Reference source not found.**. Test: M3-TMT-P4-SG1-O1-SR1-T1-N1 was selected to represent this strain rate and undergo further processing. The final analytical results need to match these test results using the same stress-strain input curve. Matching each test individually is required because each specimen has a unique geometry.
The engineering strain vs. stress relationship is derived using Equation 8 and produces the engineering stress-strain curves. Applying Equation 9 and Equation 10, the engineering stress-strain relationship is converted to true stress-strain relationship (Figure). By applying Equation 11 and adopting a Young's modulus of 210GPa, the plastic strain vs. stress relationship was calculated. To determine the necking point, the true strain vs. stress curve was smoothed and

subsequently Equation 24 and Equation 25 (differentiation stress with respect to strain) were used to obtain the tangent modulus curve. Another smoothing was performed on the tangent modulus curve, and the intersection between these two lines defined the necking point. The true stress and true strain at necking were determined. The corresponding plastic strain at necking was evaluated using Equation 21 and only the part of the hardening curve before necking was kept. By applying Equation 22, the hardening curve was extrapolated beyond necking. A total of 32 curves were generated by varying the exponent *n* between 0.1~0.5 (Figure 19). The remaining two parameters, ε_e and *k*, were calculated using Equation 25. Extrapolation was performed using MatLab.

 Each of the generated hardening curves were then input into an **LS-DYNA** *MAT_224 input deck and used to perform a simulation of the tensile test. In this model, the sample dimensions match the sample of Test M3-TMT-P4-SG1-O1-SR1-T1-N1 exactly.
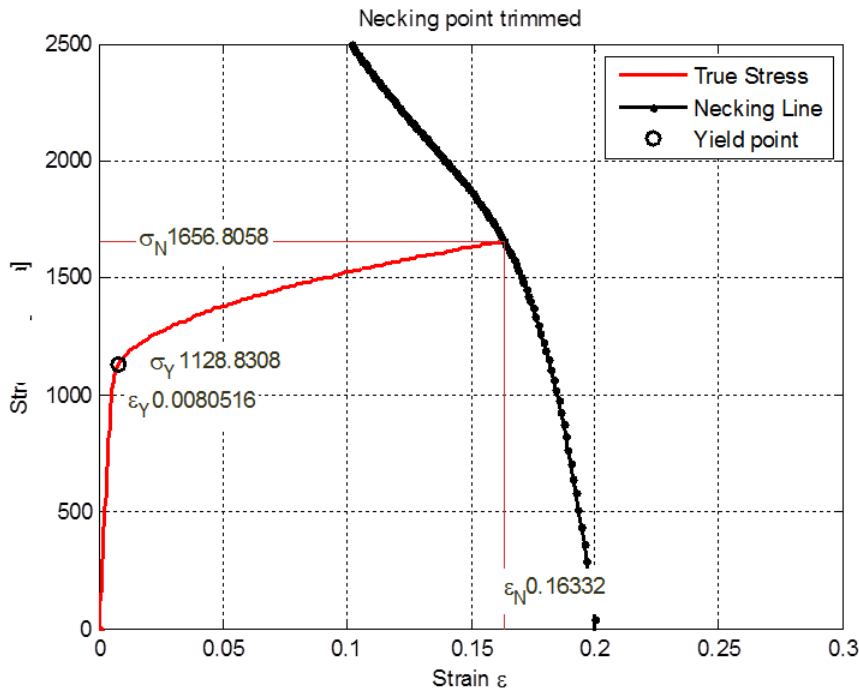

Figure 18: True Stress-Strain Relationship and Necking Point Judgment of Strain Rate = 1E-4 s⁻¹
[Test: M3-TMT-P4-SG1-O1-SR1-T1-N1]
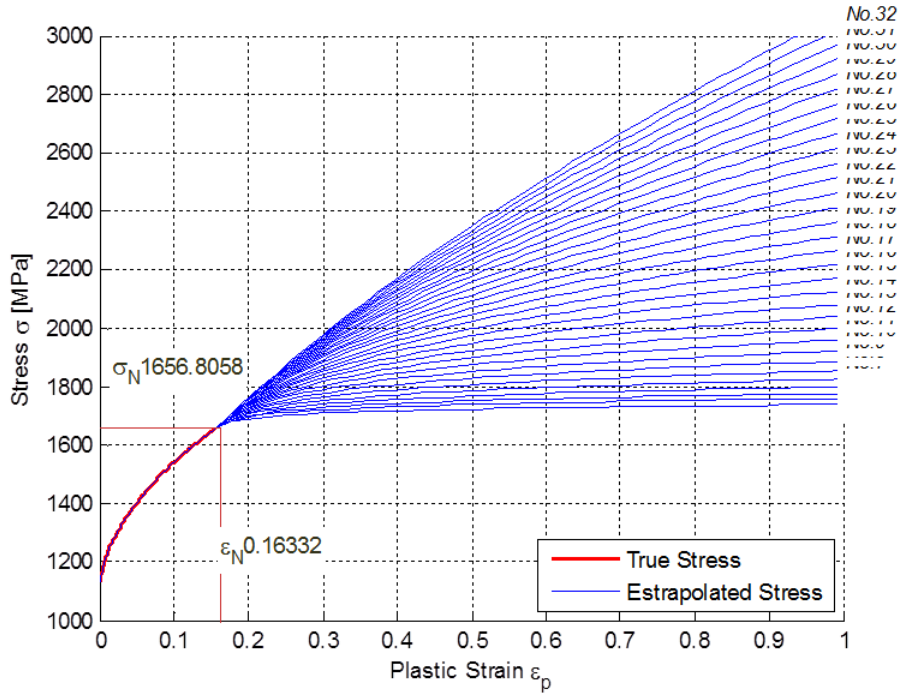
Figure 19:   Plastic Strain vs. Stress Extrapolation of Strain Rate = 1E-4 s^{-1}
[Test: M3-TMT-P4-SG1-O1-SR1-T1-N1]

As before, a cross-plot of cross-section elongation with cross-sectional force is compared to the force displacement curve from the test. This simulation is repeated for all the extrapolated candidate input curves until one of them matches the force displacement response of the test (Figure 20). A simulation contour of 1st principal strain is compared to the DIC image from the test at the time immediately before failure, with good agreement between the results (Figure).
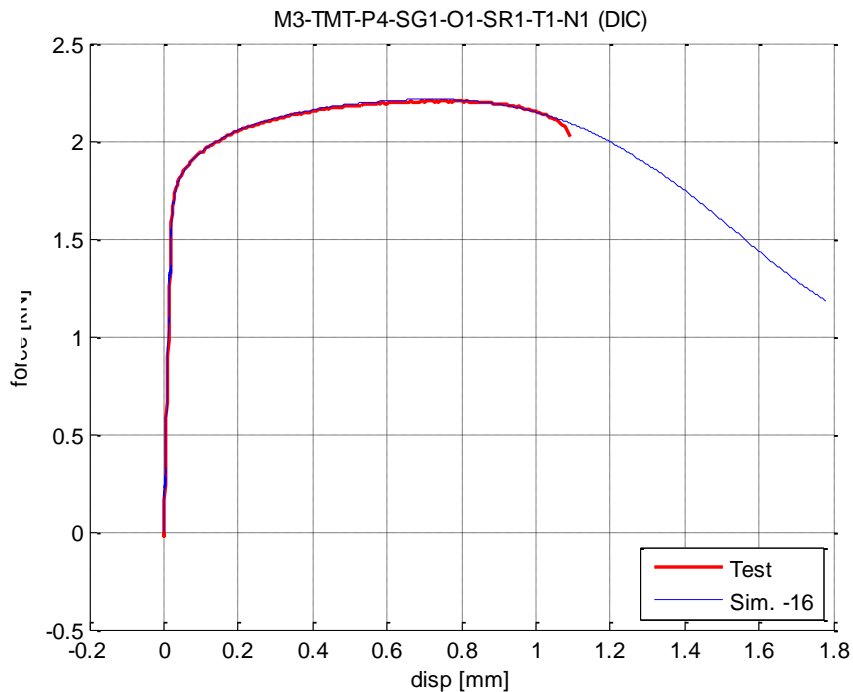
Figure 20: Force Displacement Result, Curve #16 [Test M3-TMT-P4-SG1-O1-SR1-T1-N1]
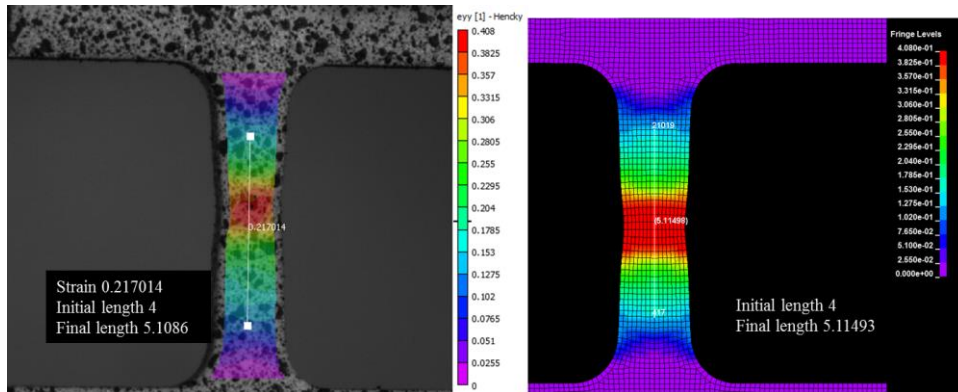
Figure 21: Left: Plastic Strain DIC Image Immediately Before Failure
Right: 1st Principal Strain Simulation Contour Immediately Before Failure
[Test 1: M3-TMT-P4-SG1-O1-SR1-T1-N1; Strain Rate = 1E-4 s^{-1}]

Stress Strain Tabulated Input of Multiple Strain Rates and Temperatures

The typical method for creating the higher strain rate curves using each high rate test, one at a time, was not feasible with Inconel-718. The *MAT_224 input curves in the iso-rate table must be at constant temperature and at a constant strain rate. Neither of these conditions was satisfied by the Inconel-718 tests, as explained previously. Also as explained before, the process employed for creating the higher rate stress-strain curves required combining information from higher rate compression tests with lower, constant strain rate tension tests. An iso-thermal constant strain rate curve needs to be used as a base-line for the synthetic high strain rate hardening curves. The stress-strain curve at the strain rate of 1E-4 s^{-1} was used as the base-line in the iso-rate table, with an off-set appropriate to match the strain rate sensitivity curve. A trial-and-error process was performed, wherein both the magnitude of the stresses in the transition and higher strain rate regions, and the Taylor-Quinney coefficient, *β*, were varied simultaneously. Each of the tests was analyzed multiple times, until a satisfactory match to all of the test data was achieved. Many iterations were performed before this satisfactory match was achieved. (Note that in Figures 23 and 24 the curve labeled 32 refers both to the simulation using the final strain rate sensitivity curve, and that 32 iterations were required before a match to all test data was achieved.)

The initial and final strain rate sensitivity curve, used to offset the base stress-strain curves, resulting from the trial-and-error process is shown in Figure 22. The final strain rate sensitivity curve shown was used to offset the base curve and to create all the iso-rate and iso-thermal input curves. Force vs. displacement, strain rate vs. strain and plastic strain DIC Image vs. principal strain rate from the simulations were also used for comparison between simulations and tests.
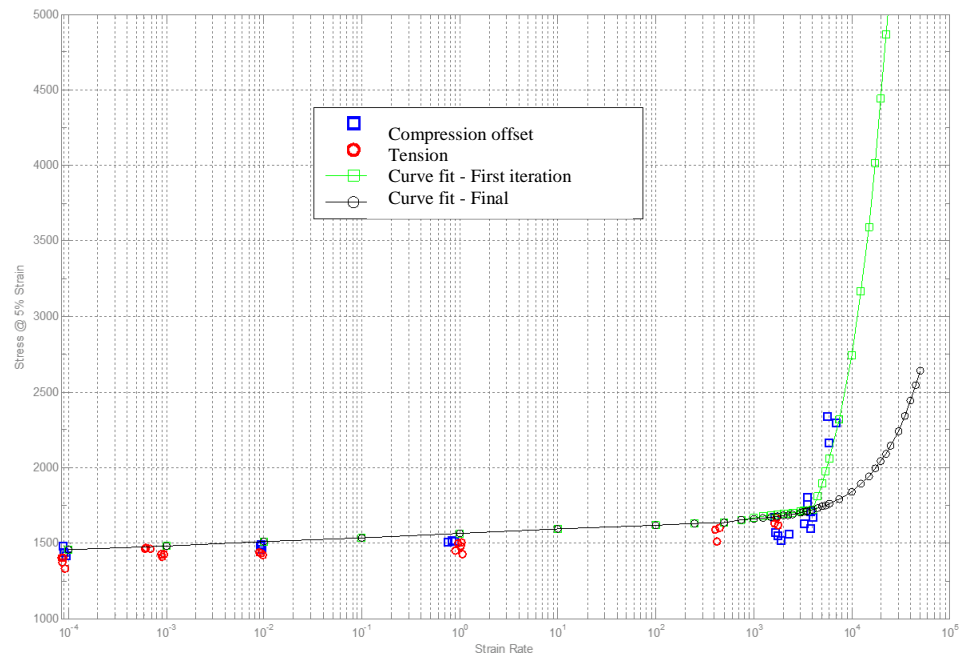
Figure 22: The Final Strain Rate Sensitivity (Stress at 5% Strain)

Stress Strain Relationship of high strain rates

These simulations were performed by applying the test displacements taken from DIC because neither of the boundary conditions of the split-Hopkinson bar tension tests was fully fixed. All six of the higher strain rate tests shown in Table 1 (nominally 500 s^{-1} and 2000 s^{-1}) were analyzed and comparisons were made to the physical test results. In the region of localization, the strain rate reached approximately 4000 s^{-1} for the nominally 500 s^{-1} test and 8000 s^{-1} for the nominally 2000 s^{-1} test.

Error! Reference source not found.23, 24 and 25 show a comparison of force vs. displacement, strain rate vs. strain and strain contour plots (DIC and **LS-DYNA®** generated) for Test: M3-TMT-P4-SG1-O1-SR4-T1-N2 (nominally 500 s^{-1}). Only one set of results is shown for space reasons. All the other simulations show a similar match to the tests.
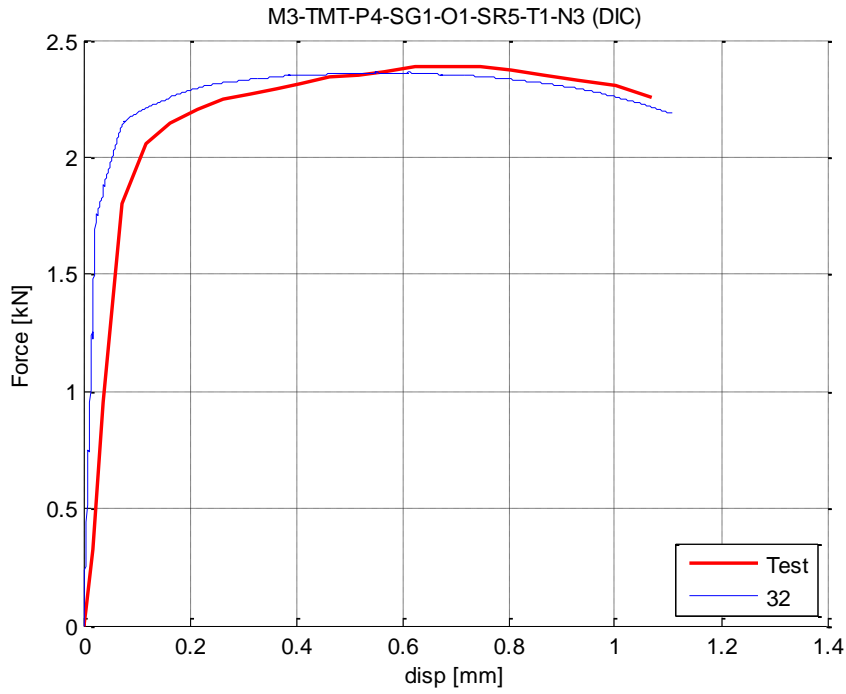
M3-TMT-P4-SG1-O1-SR5-T1-N3 (DIC)

Figure 23: Force vs. Displacement

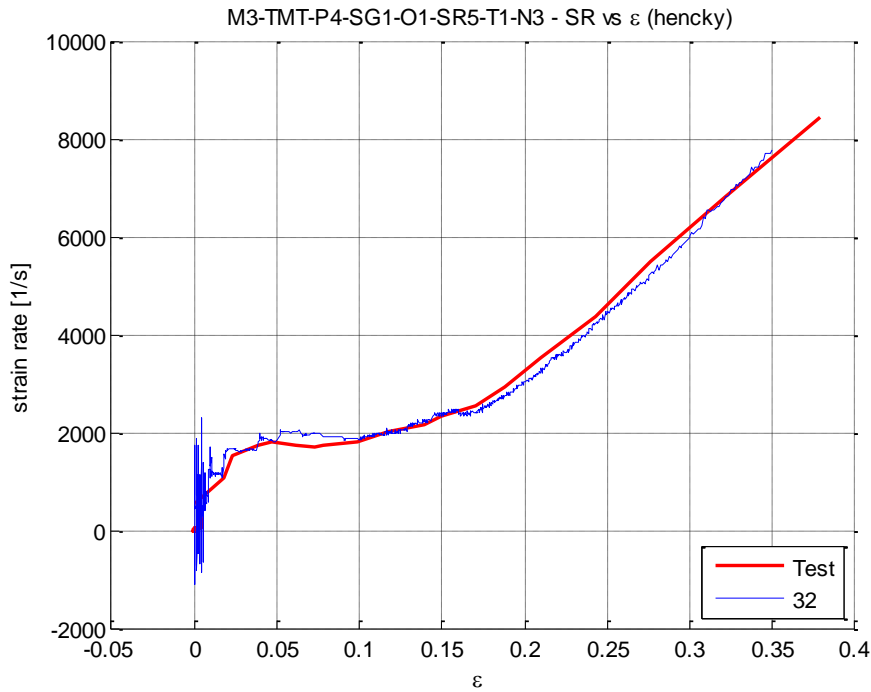M3-TMT-P4-SG1-O1-SR5-T1-N3 - SR vs ε (hencky)
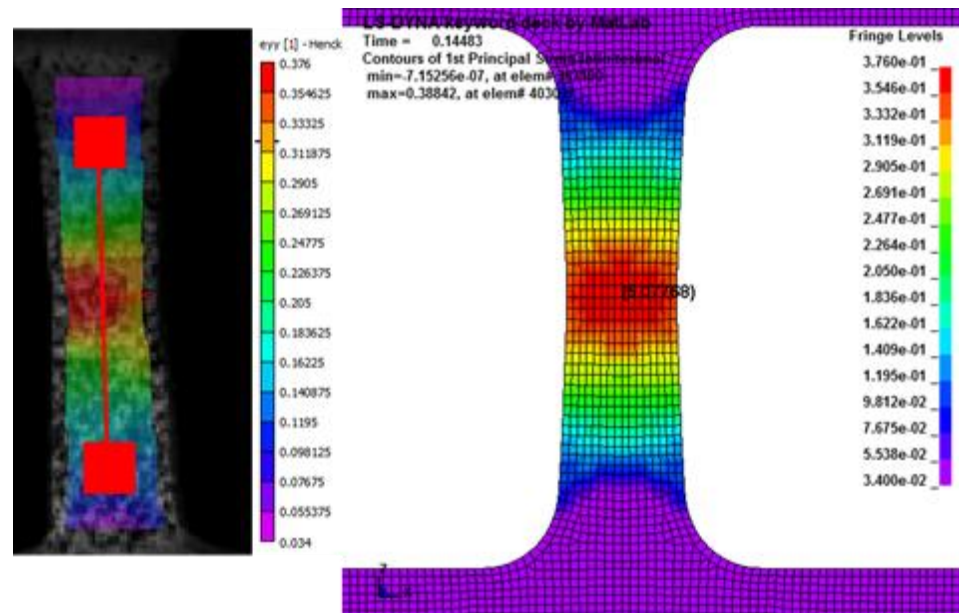
Figure 24: Strain Rate vs. strain

Figure 25: Strain Contour
[Test: M3-TMT-P4-SG1-O1-SR5-T1-N3]

Summary and Conclusions

In this paper, a complete set of material input parameters for deformation was developed and presented for Inconel-718, to be used with LS-DYNA *MAT_224. The resulting elastic-plastic material model includes strain hardening, strain rate effects, and temperature effects.
The accompanying failure surface will be developed next. It will include the effects of varying states of stress, strain rate, and temperature on the erosion failure strain. Mesh regularization to account for the effect of varying mesh densities on the failure strain will be also included.
The test samples used in the experiments were all taken from the same ½-inch Inconel plate stock. This includes samples for both the mechanical property tests and the ballistic impact tests. The mechanical property tests furnished the data that was used to create the material input parameters. Ballistic impact tests will be used to validate the model.

References

[1] *LS_DYNA Manual*, Version 971, Livermore, CA, 2007.
[2] Pereira, J. Michael, Revilock, Duane M., Lerch, Bradley A. and Ruggeri, Charles R.; "Impact Testing of Aluminum 2024 and Titanium 6Al-4V for Material Model Development", *Technical Memorandum NASA/TM 2013-217869*, NASA Glenn Research Center, Cleveland, 2013.
[3] Yatnalkar, Ravi Shriram;   "Experimental Investigation of Plastic Deformation of Ti-6Al-4V under Various Loading Conditions", B.E. Thesis, The Ohio State University, 2010. Print.
[4] Seidt, Jeremy Daniel; "Plastic Deformation and Ductile Fracture of 2024-T351 Aluminum under Various Loading Conditions", Dissertation, The Ohio State University, 2010. Print.
[5] Ressa,A.,Liutkus,T.,Seidt,J.,Gilat,A.,"Time Dependent Response of Inconel 718", *Challenges in Mechanics of Time Dependent Materials, Volume 2* 2015-12.
[6] "Tensile Strength or Tension Test", *About Civil.Org*, Web. Retrieved 2014-10-28, www.aboutcivil.org/tension-test-tensile-strength-test.html
[7] "INCONEL 718 TECHNICAL DATA", *High temp Metals*, Web. Retrieved 2016-03-02. http://www.hightempmetals.com/techdata/hitempInconel718data.php
[8] Carney, K., Pereira, M., Revilock D., and Matheny P., "Jet Engine Fan Blade Containment using an Alternate Geometry and the Effect of Very High Strain Rate Material Behavior," *International Journal of Impact Engineering,* 36 (2009) pp 720-728.

[9] Ravichandran, Rosakis, Hodowany, and Rosakis "On the Conversion of Plastic Work into Heat during High-Strain-Rate Deformation," *Shock Compression of Condensed Matter* - 2001.

[10] Rosakis, Rosakis, Ravichandran, and Hodowany, "A Thermodynamic Internal Variable Model for the Partition of Plastic Work into Heat and Stored Energy in Metals," *Journal of the Mechanics and Physics of Solids*, 48 (2000) 581-607.

[11] "AWG Modeling Guidelines Document," **LS-DYNA®** *Aerospace Working Group*, Web. Retrieved 2015-4-28. http://awg.lstc.com/tiki/tiki-index.php?page=MGD

[12] Sean Haight, Leyu Wang, Paul Du Bois, Kelly Carney, Cing-Dao Kan "Development of a Titanium Alloy Ti-6Al-4V Material Model Used in **LS-DYNA®**" DOT/FAA Report 2015-05-26.

[13] Hammer, Jeremiah Thomas; "Plastic Deformation and Ductile Fracture of Ti-6Al-4V under Various Loading Conditions", M.S. Thesis, The Ohio State University, 2012. Print.

Acknowledgments